Journal of Power Sources 254 (2014) 168–182

Contents lists available at ScienceDirect

Journal of Power Sources

journal homepage: www.elsevier.com/locate/jpowsour

A review of lithium deposition in lithium-ion and lithium metal secondary batteries

Zhe Li [a], Jun Huang [a], Bor Yann Liaw [b], Viktor Metzler [c], Jianbo Zhang [a,*]

[a] Department of Automotive Engineering, Sate Key Laboratory of Automotive Safety and Energy, Tsinghua University, 100084 Beijing, China
[b] Hawaii Natural Energy Institute, School of Ocean and Earth Science and Technology, University of Hawai'i at Manoa, Honolulu, HI 96822, USA
[c] RWTH Aachen Univ, 52062 Aachen, Germany

HIGHLIGHTS

- A review of major aspects on lithium deposition in lithium-ion and lithium metal batteries.
- Review of the deposition criteria and models that predict the occurrence of Li deposition in Li-ion batteries.
- The universality of critical potential and concentration criteria for Li deposition in Li-ion batteries is discussed.
- The morphology control is key to suppress the initiation and propagation of Li dendrites in Li metal batteries.
- Uniform, elastic and resistive SEI layers may induce favorable morphology for Li deposition.

ARTICLE INFO

Article history:
Received 23 October 2013
Received in revised form
16 December 2013
Accepted 19 December 2013
Available online 4 January 2014

Keywords:
Lithium deposition
Electrodeposition
Dendrite
Low temperature charging
Electrolyte additives
Li metal secondary batteries

ABSTRACT

Major aspects related to lithium deposition in lithium-ion and lithium metal secondary batteries are reviewed. For lithium-ion batteries with carbonaceous anode, lithium deposition may occur under harsh charging conditions such as overcharging or charging at low temperatures. The major technical solutions include: (1) applying electrochemical models to predict the critical conditions for deposition initiation; (2) preventions by improved battery design and material modification; (3) applying adequate charging protocols to inhibit lithium deposition. For lithium metal secondary batteries, the lithium deposition is the inherent reaction during charging. The major technical solutions include: (1) the use of mechanistic models to elucidate and control dendrite initiation and growth; (2) engineering surface morphology of the lithium deposition to avoid dendrite formation via adjusting the composition and concentration of the electrolyte; (3) controlling battery working conditions. From a survey of the literature, the areas that require further study are proposed; e.g., refining the lithium deposition criteria, developing an effective AC self pre-heating method for low-temperature charging of lithium-ion batteries, and clarifying the role the solid electrolyte interphase (SEI) plays in determining the deposition morphology; to facilitate a refined control of the lithium deposition.

© 2013 Elsevier B.V. All rights reserved.

1. Introduction

The lithium (Li metal) secondary battery was proposed as a high energy-density power source for high energy-demand applications in 1970s, but this battery system has remained in controversy for decades due to its vulnerability to safety and short cycle life. Continuous efforts have been made to address the most detrimental problem: the Li dendrite growth during the Li deposition in this system, which could cause capacity loss and even trigger short circuit. In recent years, although the safety and cycling efficiency have been significantly improved, this battery system has not been commercialized for large-scale applications. In contrast, the Li-ion batteries, usually having graphite as the anode in a rocking-chair configuration to facilitate the Li ions in electrode reactions, has embraced successful commercialization for portable electronic devices in the 1990s and recently for electric vehicle applications. While sacrificing the benefits of higher cell voltage and energy density of the Li metal kin, the Li-ion battery has the evident advantages in its lower risk of Li dendrite formation [1].

Fig. 1 shows two images of Li depositions on (a) a graphite negative electrode after overcharging [2] and (b) a Li metal electrode after charging [3]. In both cases, the deposited Li could grow into dendrites and cause irreversible capacity fade or even internal

* Corresponding author. Tel.: +86 10 62786918.
E-mail addresses: boryann.liaw@gmail.com (B. Yann Liaw), jbzhang@mail.tsinghua.edu.cn (J. Zhang).

0378-7753/$ – see front matter © 2013 Elsevier B.V. All rights reserved.
http://dx.doi.org/10.1016/j.jpowsour.2013.12.099

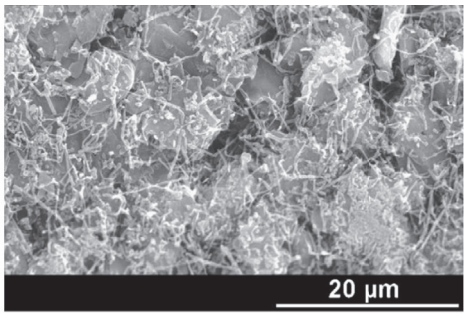

(a) An SEM image shows the Li deposition on a graphite negative electrode after overcharging [2].

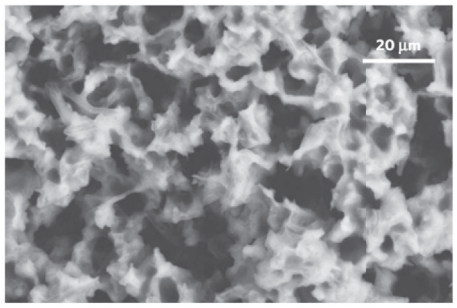

(b) An SEM image exhibits the Li deposition on a Li metal electrode after charging [3].

Fig. 1. Images of Li deposited at the negative electrodes (graphite and Li metal respectively).

short. However, despite the similarity of such detrimental effects, the Li deposition phenomena are essentially different in secondary Li metal and Li-ion batteries since the depositions occur under different working conditions.

For the Li-ion battery with the graphite anode, under normal working conditions (i.e. the cycling rates, temperature and cut-off voltage in the nominal range), Li ions intercalate into or de-intercalate from the active materials reversibly between the two electrodes. Only under harsh charging conditions such as over-charging or charging at low temperatures, the Li ions could be reduced to metallic Li and deposit as an interphase. Therefore, to study the Li deposition phenomenon in Li-ion batteries, the electrochemical models, which are based on the mechanism and electrochemical kinetics of Li deposition with specific criteria, should be helpful in providing quantitative understanding of this phenomenon. The application of these electrochemical models would allow us to quantify the criteria to prevent or mitigate the occurrence of Li deposition during cycling. The model could provide solutions in two aspects: (1) improvements in battery design, electrode architecture and material property and (2) developments of appropriate charging protocols for commercial chargers.

For the Li metal secondary battery, Li deposition/dissolution is an inherent process at the interface of Li metal/electrolyte during normal cycling. The deposited Li could form several types of surface morphology: including moss-like, particulate (granular), or dendritic (needle-like) deposits. The dendritic aggregation is the most detrimental to the cycling efficiency and battery safety since dendrites could accelerate the capacity fade due to the formation of electrically isolated Li ('dead Li'), or even trigger the internal short when piercing through the battery separator. Therefore, unlike aiming at the inhibition of Li deposition in the Li-ion battery, the morphology control of the Li-deposited surface is key to successful development of the Li metal secondary battery. The formation of dendrites should be minimized or eliminated, and the deposited Li should be confined to less harmful, smoother microstructure with mossy or particulate morphologies. The key aspects of Li deposition in the Li-ion and Li metal secondary battery systems are compared in Table 1.

The Li deposition in both battery systems is reviewed in this paper. For the Li-ion battery, the electrochemical kinetic models are investigated, and the threshold condition control and measures, including novel charging protocols, are evaluated. For the Li metal secondary battery, the dendrite propagation models elucidating the dendrite initiation and simulating the growth are discussed, and the attempts to suppress dendrite propensity are presented, mainly on the electrolyte modification and the working condition control. In the end, resulting from the survey of the literature, emerging research areas for further studies are suggested.

2. The Li deposition in Li-ion batteries

The mechanistic models of Li deposition in Li-ion batteries are summarized in Table 2. Subsequently, several optimization theories for ideal charging protocols are reviewed. Since most of the theoretically optimal charging methods are difficult to implement in practice, we shall focus on practical charging methods, which may be good approximations to the theoretical optimal methods for easy adoption by commercial chargers.

2.1. The mechanistic models and criteria of Li deposition in graphite electrodes

The mechanistic models describing the ion concentration and current distribution based on diffusion laws and conservation equations can predict the timing of deposition occurrence with the proposed criteria. From the perspective of the deposition criteria, the models of Li deposition in Li-ion batteries are listed in Table 2.

Purushothaman and Landau [4] predicted that Li would accumulate at the interface of the negative electrode and the electrolyte during charging when the Li flux of charge transfer reaction at the graphite/SEI interface was higher than the Li diffusion flux into the graphite particles. This interfacial accumulation would eventually lead to the dendritic growth when the Li ion concentration at the interface exceeded the saturation level of 0.077 mol cm^{-3}. Based on

Table 1
Comparisons of the Li deposition in Li-ion and Li metal batteries.

Item	Li-ion battery	Li metal battery
Normal reaction at negative electrode during charging	$xLi^+ + 6C + xe^- \rightarrow Li_xC_6$	$Li^+ + e^- \rightarrow Li$
Li deposition circumstances	Overcharging or charging at low temperatures	Normal charging
Focus	Threshold condition control	Surface morphology control
Description model	Electrochemical kinetic model	Dendrite propagation model
Controlling factors	(1) Battery design (2) Electrode architecture and material property (3) Charge protocol	(1) Battery components (2) Current density (3) Temperature, pressure and external interference

Table 2
The models of Li deposition in Li-ion batteries.

Criterion	Model	Macro-dimension	Main assumptions
A Saturation concentration at the interface	Purushothaman et al., 2006 [4]	One-dimensional (through-plane direction)	The mass transport controls the charging process.
The interfacial overpotential equals to zero vs. Li/Li^+	Arora et al., 1999 [5]	One-dimensional (through-plane direction) or pseudo two-dimensional (plus the particle radius micro-direction)	The same as the Doyle–Fuller–Newman pseudo two-dimensional porous electrode Li-ion battery model [6] (referred as DFN assumptions below)
	Tang et al., 2009 [7]	Two-dimensional, considering the edge effect of electrode (through-plane and in-plane direction)	Table 2 in Ref. [7]
	Perkins et al., 2012 [8]	One-dimensional (through-plane direction)	(1) DFN assumptions; (2) Batteries in a quasi-equilibrium state, neglecting local variations in the concentration of electrolyte and the solid surface

Table 3
The impact of design parameters on Li deposition in Li-ion batteries.

Impact factor	Correlation
C/A ratio	Lower C/A ratio suppresses the deposition but compromises on the capacity retention during the formation process (or the first cycle) [5,7].
Excess of negative electrode length	Extending the negative electrode beyond the positive electrode delays the onset of Li deposition. In the modeling of Ref. [7], an extension of 0.4 mm in the negative electrode could eliminate the Li deposition before the cutoff voltage is reached. In addition, to conserve the capacity by simultaneously extending the negative electrode and making it thinner has few impacts on delaying the deposition before the cutoff voltage is reached [7].
Negative electrode thickness	Making the negative electrode thicker is beneficial to the inhibition of Li deposition since it reduces the C/A ratio. However, at a fixed C/A ratio, it is less effective than extending the negative electrode length [7]. In addition, if the C/A ratio is conserved while changing the thickness of both electrodes, the battery with thicker electrodes is more prone to Li deposition [5].
Separator thickness (inter-electrode distance)	In the range of appropriate C/A ratio, which is realized by extending the negative electrode length, a longer inter-electrode distance (or a thicker separator) is more effective in preventing deposition [7].

the criterion of concentration saturation and the assumption of mass-transport limiting step, they optimized the current profiles for rapid charging (details in Section 2.3.3).

In 1999, Arora, Doyle, and White first proposed a Li deposition model for a $C/LiMn_2O_4$ battery [5] based on the Doyle–Fuller–Newman model of Li-ion batteries [6], which is a macroscopic one-dimensional or pseudo two-dimensional model for porous electrodes. This model divided the current density of the carbon-based electrode into two parts, the Li intercalation current and the Li deposition current, and related the Li deposition current to the potential of Li deposition reaction through the Butler–Volmer equation. The interfacial overpotential of Li deposition reaction vs. Li/Li^+, $\eta_{Li/Li+}$, was expressed as:

$$\begin{cases} \eta_{Li/Li+} = \phi_n - U_0 \\ \phi_n = \phi_s - \phi_e - Fj_nR_{SEI} \end{cases} \quad (1)$$

here, ϕ_n is the potential across the SEI layer with respect to the deposition reaction, ϕ_s,ϕ_e the potentials in solid and electrolyte phase respectively, U_0 the open circuit potential of the Li deposition reaction (Li/Li^+), j_n the pore wall flux of the Li deposition reaction, R_{SEI} the SEI layer resistance, and F the Faraday constant.

In this model the deposition criterion was set as $\eta_{Li/Li+} < 0$. With this criterion, this model correlates the propensity of Li deposition to the profiles of ion concentration and current density in the vicinity of the electrode interface, and enables the prediction of the exact time when the Li deposition would occur, given a specific charging waveform and ambient condition.

In 2009, the Arora model was extended by Tang, Newman, et al. [7] using a macroscopic two-dimensional model to address the current distribution profiles in both through-plane and in-plane directions. The authors stated clearly that the Li deposition could be triggered by either $\eta_{Li/Li+} < 0$ or the concentration saturation at the interface. The potential criterion was adopted in their model to consider the impact of edge effects on the Li deposition and discuss the appropriate length ratio of the positive and negative electrodes.

In 2012, the Perkins reduced-order model [8] simplified the Arora model by a quasi-equilibrium assumption. The simplified model achieved satisfactory accuracy while reduced the actual computation load down to less than 1/5000 of that of the original model. It should be noted that the Perkins model is generally applicable to a single charging pulse shorter than 10 s or alternating charging–discharging pulses in which the cumulative change of the state of charge (SOC) remains minimal, e.g. the real time control of the hybrid power systems, since the model is established on a quasi-equilibrium assumption. The authors of this reduced-order model have proved that continuous long-term charging or pulse charging with a length much greater than 10 s could yield significant mismatch between the Arora and the Perkins models.

2.2. The impact of battery design and material property on Li deposition in Li-ion batteries

2.2.1. Battery design

Battery design has a considerable impact on the Li deposition in Li-ion batteries. Table 3 summarizes the battery design parameters that have been shown to have an impact on the Li deposition either by experiment or simulation [5,7]. Among these parameters, increasing the negative active material excess (i.e. decreasing the C/A ratio) or extending the negative electrode beyond the edge of the positive electrode even by approximately 1 mm can significantly delay the occurrence of Li deposition. However, since the excess

Table 4
The impact of material properties on Li deposition in Li-ion batteries.

Impact factor		Correlation
Kinetic parameters related to material property	Exchange current density	Higher exchange current density accelerates the rate of Li deposition and depletes the Li ions in the system sooner [5].
	Reaction rate constant in the negative electrode	Deposition is extremely sensitive to this constant, and higher reaction rate suppresses the Li deposition dominantly rather than geometry parameters [7].
	Electrolyte conductivity	Increasing the conductivity is beneficial to the delay of the Li deposition, but the correlation is considerably weak. (In Ref. [7], a factor of 4 increase in the conductivity delayed the Li deposition for only 10 s).
Material property of negative material	Particle size	The battery with larger negative particles is prone to Li deposition [5].
	Surface disorder/crystallinity /graphitization	See '*Note 1*' below.
	Particle shape	The deposition is more likely to occur in graphite with the shape of flake or fiber than with smooth round-shaped outlines. See '*Note 2*' below.

Note 1: Surface disorder/crystallinity/graphitization of the negative material.
It was indicated [2] that the increased disorder of the graphite surface (measured by the R-value to reflect the degree of graphite crystallinity) caused more deposition on the surface but suppressed the formation of dendrites. Although the increase of defects on the disordered graphite provided more nuclei for electrodeposition and induced more deposition on the surface, the deposition was more likely in granular shapes since the multiple nuclei on the surface disturbed the formation of dendrites. Five types of graphite materials in different graphitization degrees and particle shapes were compared in Ref. [9] at room temperature and −5 °C. No apparent correlation between the Li deposition propensity and the material graphitization was observed at either room temperature or −5 °C. However, it was discovered that batteries with higher graphitization or better surface crystallinity were affected more greatly, and the amount of Li deposition on the surface was increased more significantly at low temperatures.
Note 2: The particle shape of the negative material.
It was indicated in Ref. [9] that the deposition was more likely to occur in the graphite with particles in the shape of flake or fiber compared with the particles in the shape of spheres, since the particles with smooth outlines facilitated the Li-ion intercalation and mitigated the Li accumulation at the SEI. Meanwhile, Ref. [10] pointed out that the capacity retention at low temperatures was improved and the Li deposition was suppressed after the natural graphite was treated by 10% wt. carbon coating. This improvement was explained by the scanning electron microscope (SEM) imaging, which clearly showed that the particles of the negative material had transformed from a flake-like shape to circular shape after the carbon coating. Further X-ray diffraction (XRD) results reinforced the judgment about the impact of the particle shape: after charged at low temperatures, an obvious content of LiC_{12} and Li metal was detected in the natural graphite without coating, whereas no LiC_{12} and little Li metal were detected in the carbon-coated material. The lower content of LiC_{12} and Li metal in the carbon-coated material proved evidently that the smooth shapes of material particles facilitated the migration of Li ions into the depth and significantly inhibited the Li deposition.

either in the material mass or in the length of the negative electrode could result in large capacity loss during the first cycle, the C/A ratio and the length of the negative electrode should be cautiously optimized.

2.2.2. Material property

The kinetic parameters in both solid and electrolyte phases, which are determined by the material property and assembly quality, have a major impact on the Li deposition. Furthermore, the microstructure of the negative electrode material, including the lattice structure and the particle shape/size of graphite, also affects the characteristics of Li deposition, as shown in Table 4.

2.3. The optimization theory of ideal charging profiles

2.3.1. The J.A. Mas empirical optimal charging based on the acceptable current

An empirical optimal charging curve was proposed by Mas in 1970s [11–13] to charge the battery at an acceptable rate, which was defined as the maximum current that would not induce gas production in aqueous batteries. After massive tests on Pb-acid and Ni–Cd batteries, the acceptable current was described empirically in an exponentially decaying relationship with the charging time, as shown in Eq. (2):

$$i = I_0 \exp(-at) \tag{2}$$

where I_o is the initial current, a is the acceptance ratio that determines the rate of current decay, t is the charging time. For a specific battery system, the acceptance ratio, a, is a function of the depth of discharge (DOD) and the rate of the preceding discharge. The acceptance ratio is characterized by three empirical laws with respect to the discharging history:

(1) The acceptance ratio of a battery is inversely proportional to the square root of the DOD in the preceding discharge. The acceptance ratio of a battery varies linearly with the logarithm of the rate in the preceding discharge.

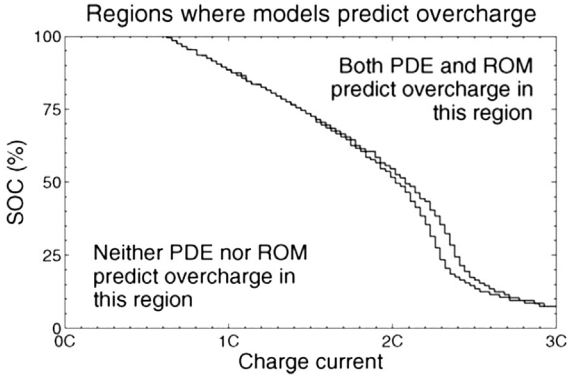

Fig. 2. The optimal pulse charging protocols [8] based on the Arora model (PDE) and the Perkins reduced-order model (ROM).

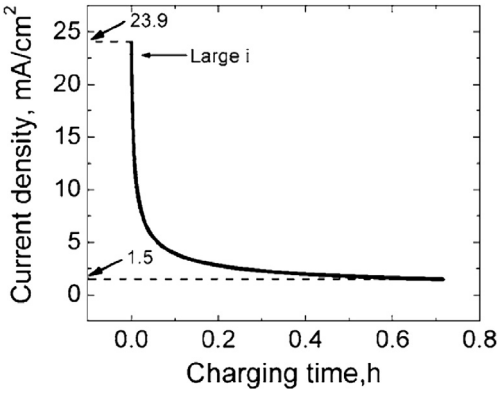

Fig. 3. The optimal charging current profile based on the hypothesis of maintaining saturated Li concentration at the electrode/electrolyte interface [4].

Table 5
Various types of practical charging protocols in the literature.

Charging method	Protocols	Refs.
Constant current-constant voltage (CC–CV)	Charged with a constant current till a voltage limit is reached, and then charged with this voltage till the current drops to a preset value.	[14–16]
Multistage CC (MCC)	Charged with stepwise descending currents	[17]
Varying current decay (VCD)	Charged with continuous descending currents	[18,19]
Boost charging	Pre-charged with a constant voltage V_I, and then switched to CC–CV charging with V_{II} as the voltage limitation ($V_I > V_{II}$)	[20]
Pulse charging	Charged with charging/discharging current pulses (usually in rectangular waveforms)	[4,11,12] [13,21,22]
Sinusoidal ripple current (SRC) charging	Charged with alternating sinusoidal currents	[23]
Feedback charging	Charged by the feedback control based on the residual energy evaluation	[24]
Preheating charging	Preheating the battery with alternating charging and discharging at low temperatures	[25–27] [28,29]

Table 6
The influencing factors in the CC–CV charging protocol.

Item	Influencing factor	Correlation
Protocol design related (given fixed cut-off voltage)	Ambient temperature	Low temperature could result in the Li deposition, prolong the charging duration, and reduce the charging energy efficiency [14].
	CC current	Increasing the current does not reduce the charging time significantly once the current reaches a certain level. This is because it could aggravate the polarization, induce the Li deposition, and decrease the proportion of the capacity increase in the CC stage [14,15].
Battery design related	C/A ratio	A small C/A ratio suppresses the Li deposition in the CC–CV charging [14].
	Positive electrode thickness	The charging time of the CC–CV method is increased in proportion to the positive electrode thickness [16].
	Negative electrode thickness	The thickness of the positive electrode is more important than the negative [16].
	Separator thickness and porosity	Thinner and more porous separator reduces the charging time slightly [16].
	Tab width	Tab width is not effective in reducing the charging time [16].
Material property related	Ion diffusion coefficient	Larger ion diffusion coefficient increases the charging efficiency [15].
	Composition and salt concentration of electrolyte	See more details in Tables 3 and 4 of Ref. [16].
	Particle size of active material	Smaller particle size increases the charging efficiency [15].

(2) After discharged at several different rates, the overall acceptable current is the sum of the acceptable current under each discharge rate.

Based on this empirical optimal curve, several charging methods have been proposed and the corresponding apparatuses created. Intermittent discharging pulses are coupled into the charging current to produce desirable charging profiles.

2.3.2. The optimal pulse charging based on the Arora and Perkins models

The optimal pulse charging was suggested in Ref. [8] based on the Arora model [5] and the Perkins reduced-order model [8], as the contours in Fig. 2 show. The contours define the regions of the SOC and the pulse amplitude where deposition would and would not occur when the cell were charged with 1 s current pulses separated with 0.2 s rest intervals. When the pulse charging sequence follows the contours in Fig. 2, the maximum charging rate should be achieved under the condition of no Li deposition.

2.3.3. The optimal charging based on the hypothetical maintenance of saturated interface concentration

The maximum Li ion concentration at the interface of the negative electrode/electrolyte, which should result in no Li deposition, was assumed in Ref. [4] as a constant for a specific battery system. With the hypothesis of maintaining this saturated Li ion concentration throughout the charging process, the optimal charging profile can be achieved for continuous charging. If the charging were carried out in accordance with this optimal waveform, the maximum charging rate should be realized without Li deposition. Since the diffusion rate of Li ions in the graphite lattices decreased with the continuous intercalation of Li ions in the charging process, it was concluded that the current amplitude of this optimal waveform should be kept decreasing to ensure that the Li ion concentration at the interface would not exceed the maximum value allowed before triggering the Li deposition. Therefore, the optimal charging current profile exhibits a nonlinearity of decrease, as shown in Fig. 3.

2.4. The evolution of practical charging protocols

The charging theories have led to several optimal charging profiles, which ensure the maximum charging rate achieved with no Li deposition. Most of these profiles are strongly dependent on battery specifications, presented in nonlinear or even random waveforms, and difficult for commercial chargers to implement. Various practical charging protocols, which approximate the effect of ideal charging profiles easily adopted by commercial chargers, have been extensively reported in the literature and summarized in Table 5.

The CC–CV charging method has been extensively used in commercial chargers due to its ease to implementation. The main problem with this widely used method is that it takes a long time (mainly in the CV stage) to fully charge the battery, hence hampering the convenience of the electric vehicles even under fast charging mode. Moreover, the Li deposition has been repetitiously observed in the late stage of the CC–CV charging, especially at low temperatures or when the initial CC charging rate is high. Multiple

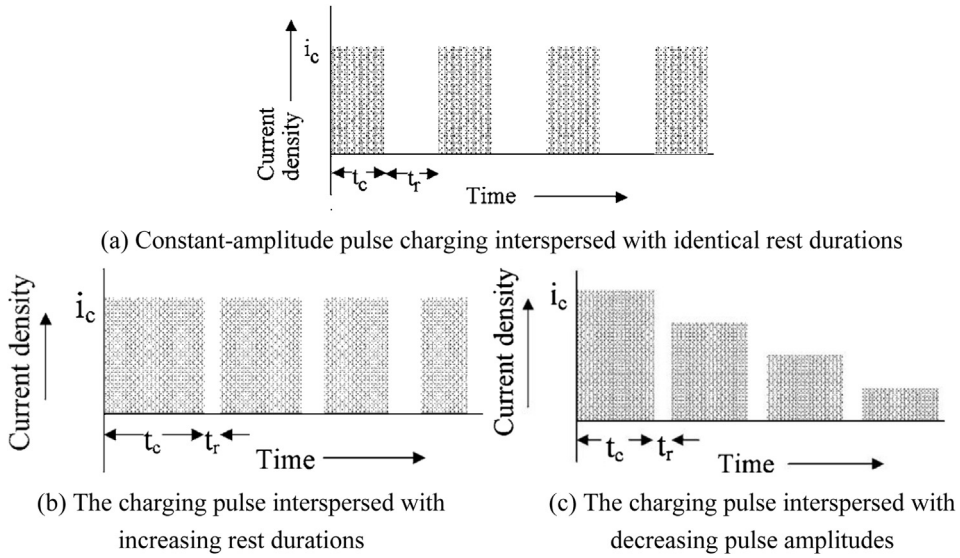

Fig. 4. Different parameter settings of pulse charging [4] waveforms that have been proposed to increase charge efficiency or reduce charging time.

influencing factors in this CC–CV charging method, either on the protocol or the battery design, are categorized in Table 6. The correlations between these factors and the efficiency of the charging method are also presented.

To relax the polarization and the propensity of Li deposition in CC–CV charging, the MCC method was proposed to charge the battery with a sequence of stepwise descending currents. The ant colony system (ACS) algorithm, which had been developed to solve the constrained combinatorial problems, was adopted in Ref. [17] to determine the magnitude of each current step in MCC charging profiles.

The basic intension of the VCD charging method is quite similar with MCC. The major difference is that the VCD method charges the battery with a continuous and monotonic descending-current instead of the stepwise current in MCC. A linearly decreasing charging current profile was used in Ref. [18] and the charging time was significantly reduced compared with constant current charging. A nonlinearly decreasing current profile in an empirical form of Eq. (3) was used to compare between the VCD and traditional CC–CV charging methods [19] in a few different types of batteries, and the electrochemical impedance spectroscopy (EIS) characteristics of two electrodes as well as the microscopic morphology of material particles were considered.

$$I(t) = \frac{I_0 + k_1 t^{1/2}}{1 + k_2 t^{1/2} + k_3 t} \tag{3}$$

where k_1, k_2, k_3 are arbitrary constants (optimized for a specific chemistry and cell design), I_0 the initial current, and t the instantaneous time.

The boost charging method was introduced in Ref. [20], the signature of which was a CV pre-charging stage before the CC–CV stage started, as illustrated in Table 5.

In recent years, the pulse charging method has aroused widespread interests due to its advantage on shortening charging time as well as preventing battery aging. In Ref. [21], it was shown that pulse charging, which involved short relaxation periods or short discharge pulses during charging, could improve the energy efficiency and the cyclic voltammogram characteristics compared with CC charging. Battery EIS and material SEM/XRD results provided further proof that this pulse charging method also helped to improve the structural stability of the cathode material and to reduce the impedance accumulation of the negative electrode.

In Ref. [4] the impacts of different parameter settings on the effectiveness of pulse charging were compared. Pulse charging with constant pulse amplitudes and constant rest durations (Fig. 4(a)) was proved not useful to accelerate the charging process since this type of waveform had little effect on the relaxation of the ion accumulation at the solid/electrolyte interface, which was believed to be the rate-limiting step of fast charging. On the contrary, continuously lengthening the rest duration (Fig. 4(b)) or reducing the amplitude of charging pulses (Fig. 4(c)) was able to effectively relieve the Li ion accumulation at the interface and accelerate the charging process.

Although J.A. Mas has proposed the optimal exponentially descending current profile in the patents [11–13], he alternatively realized a more practical charging profile in the design of charging circuit as disclosed in these patents. The preferred charging profile was interspersed by discharging pulses, and the rate and duration of which varied in accordance with the relative magnitudes of the maximum acceptable charging current.

Some other novel charging methods have been proposed to reduce the charging time and eliminate the side effects, including the sinusoidal alternating current (AC) charging [23] and the feedback-control charging [24].

In particular, a pre-heating charging method has been proposed to address the Li deposition propensity at low temperatures. Stuart and Hande published a series of patents and papers from the year 2001–2004 on their design of a high frequency battery heating circuit [25–27], which was used to heat the battery by AC in cold climates before the battery pack was substantially charged. For a battery pack (Panasonic NiMH batteries, 128 V, 6.5 Ah, SOC = 55% connected in series) soaked at −20 °C, it was possible to heat the pack to room temperature within 6–8 min by circulating a 10–20 Hz 60 Arms AC. Furthermore, they investigated the influences of different current amplitudes and battery SOCs on the temperature rising rate and found that the heating process was accelerated when either the current amplitude was increased or the battery SOC was high. Pesaran et al. [29] commented that heating battery internally by AC could result in not only the fastest heating speed under the same heat input but also the most uniform temperature distribution in comparison with the external jacket heating or the

airflow heating. Furthermore, they indicated that applying the high frequency AC heating could heat up the battery with less damage and energy loss than the direct current (DC) heating. This preheating measure has recently been discussed for its application to the battery thermal management system (BTMS) in the electric vehicles used in the regions with cold winter [30].

3. The Li deposition in Li metal secondary batteries

Since the first observation of the dendritic deposition of Li in 1980s [31], the morphology of the Li deposition has been extensively studied; especially in the areas of modeling and suppression of the dendrite growth in Li metal secondary batteries. In this section, the models of dendrite initiation and propagation are summarized, focusing mainly on but not limited to the Li deposition. The mechanism of the Li deposition process, including the conditions of the dendrite formation, is presented. The desirable characteristics of the SEI layer on the negative electrode, which is supposed to dominate the deposition morphology, are discussed. Subsequently, the multiple factors affecting the SEI quality and the deposition morphology are categorized. Finally, the observation methods of the electrode surface employed in the study of deposition morphology are presented.

3.1. Models describing dendrite initiation and propagation

3.1.1. The surface-tension model

The first comprehensive model was proposed by Barton and Bockris [32] to study the conditions for dendrite initiation and growth velocity of silver deposition in well-supported liquid electrolytes. In this model, the surface tension was assumed to be one of the driving forces of dendrite propagation, and it could be calculated by its correlation with an overpotential term caused by pressure variation inside and outside the dendrite tip. This model predicted a parabolic shape of dendrite tip where the next deposition was preferred due to the enhanced spherical diffusion rate.

Diggle et al. [33] extended the Barton surface-tension theory to the Tafel region of overpotential and presented a detailed description of the initiation mechanism.

The modeling work by Monroe and Newman [34] applied the Barton and Bockris surface-tension model to Li/polymer systems. After calculating the concentration and potential profiles of a parallel-electrode system, they derived the one-dimensional model for an isolated needle-like dendrite. This derivation was done under the assumptions that the tip was static and in a hemispherical shape, without considering the viscous and mechanical forces. A propagation behavior similar to that in the well-supported liquid systems was attained. In a subsequent paper, Monroe and Newman [35] developed the model to include the elasticity, viscous drag, and mechanical pressure as additional influencing factors, and their effects on the exchange current density and the potential profile were then discussed.

In this type of surface-tension models, the dendrite growth was divided into two stages: the initiation and the propagation.

(1) The initiation stage

Barton and Bockris [32] suggested that in the initiation stage, the tip formed its own spherical diffusion layer out of the global linear diffusion and the preliminary prismatic protrusions grew through the diffusion layer of the substrate. A critical current density and overpotential (3 mV in Ref. [32]) for the initiation have been determined as a function of the solution purity and the ion concentration.

Diggle et al. [33] distinguished two different initiation-related times. The first initiation time τ_i is the time when dendrites are clearly visible in experiments. The other initiation time τ_d represents the time when dendrites are initiated but still invisible in experiments. This initiation time to create critical embryo that can grow into a dendrite τ_d could be obtained by extrapolating the 'dendrite-length vs. τ_i' plot to the zero dendrite length (usually, $\tau_d < \tau_i$). The initiation time τ_d also represents the time required to attain the necessary stable radius of the curvature for the spherical diffusion at the tip.

(2) The propagation stage

After the initial stage, the velocity of the dendrite propagation, v, is related to the current density, i, as described by Barton and Bockris [32] in Eq. (4):

$$v = \frac{iV}{F} \tag{4}$$

where V is the molar volume of dendrites, and F the Faraday constant. They expressed the total overpotential in Eq. (5), which takes into account the activation overpotential (η_a), the diffusion overpotential (η_d) and the surface-tension-related overpotential (Δe_r).

$$\eta = \eta_a + \eta_d + \Delta e_r \tag{5}$$

where $\eta_d = irRT/Dc_\infty F^2$, $\Delta e_r = 2\gamma V/Fr$, γ is the surface tension between the metal and the solution, r the tip radius, D the ion diffusion coefficient, c_∞ the ion concentration in the bulk solution, T the temperature, and R the gas constant.

Based on Eqs (4) and (5), the effects of the overpotential, ion concentration and temperature on the velocity of the dendrite propagation were discussed in Refs. [32,33]. It was deduced from Eq. (5) that there existed an optimal radius r_{opt}, at which the growth rate was maximized under a specific overpotential and ion concentration. It was further concluded that $v \propto \eta$ under a low exchange current, and $v \propto \eta^2$ under a high exchange current.

In the propagation stage, the morphological stability analysis of dendrites was first deduced by Barton and Bockris [32]. A more general theoretical stability analysis of dendrites was presented by Mullins and Sekerka [36,37], and the analysis was later used by Aogaki and Makino [38] to analyze the stability of electrodes in the diffusion-limited electrodeposition.

3.1.2. The Brownian Statistical simulation model

Modified from the classical diffusion-limited aggregation model [39], the Brownian statistical simulation model has become a useful approach to simulate the morphology evolution of the deposited species. The general procedures to simulate the morphology evolution are described as follows: (1) a single mobile ion [40,41] or multiple mobile ions [42–47] are randomly distributed in the simulation domain. An active region [42] and some randomly distributed active sites [44] at which the deposition allows are preset. (2) The mobile ions are designed to move randomly (such as in Brownian motion [44,45]) in the simulation domain under specific boundary conditions. The effect of electromigration and convection could also be incorporated into this model [47]. (3) When the mobile ions arrive at the active sites, the deposition probability of these ions P_s is defined to represent the balancing between the rate of the electrochemical reaction and the bulk diffusion [42–46]. The deposition probability is assumed as unity in the diffusion-limited model of deposition aggregation. The determination of P_s is sophisticated since the value depends on multiple parameters like the overpotential, the limiting current, the exchange current

density and the bulk electrolyte concentration. Voss and Tomkiewicz [42] derived the first specific equation to present the correlation between P_s and these parameters. Mayers et al. provided another expression of P_s in Ref. [46]. (4) With the hypothesis of the stochastic motion and the definition of the deposition probability, the morphology evolution of the dendrite aggregation is simulated statistically.

Magan et al. [44] extended the dimensionless simulation models in the previous work to a real physical model both on temporal and spatial scales, investigated the impact of the deposition probability on the size dispersion of interfacial nanostructures, and concluded that reducing the probability was effective to reduce this size dispersion. In a subsequent work, Magan et al. [45] applied this model to characterize the deposition structure quantitatively by various morphological parameters. Recently, Mayers et al. [46] introduced this model to rechargeable Li metal secondary batteries and successfully suppressed the dendrite propagation with pulse charging. Besides, they clearly indicated that the deposition morphology was determined by a competition between the timescales of the cation diffusion and the reductive deposition at the interface.

Under a low deposition probability, the diffusion is more extensive than the reductive deposition, and Li ions have more chances to penetrate into the depth and deposit in the vicinity of the substrate, which results in a dense deposition structure and a low propensity of dendrite formation. On the contrary, a relatively high deposition probability increases the possibility of deposition in the tip of the existing deposition bush, which should lead to a diffuse deposition structure and a high propensity of dendrite formation.

The Brownian statistical simulation model smartly correlates the macro-scale dendrite morphology evolution with the diffusion intensity and the electrochemical reaction probability. The main drawbacks of this method are the time-consuming simulation process and the underlying difficulty in the precise determination of the deposition probability. Additionally, for porous electrodes such as in Li-ion batteries, since Li ions can penetrate into the active particles and transport inwards, some significant modifications should be made before applying this model to simulate the deposition morphology in this type of system.

3.1.3. The Chazalviel electromigration-limited model

Developed in 1990s, the Chazalviel model described the dendrite initiation induced by an electrodeposition process, which was limited by electromigration other than diffusion. In Ref. [48], the ion concentration and potential profiles were calculated in an electrochemical system made of two copper electrodes immersed in aqueous $CuSO_4$ electrolyte. It was concluded that, when a high electric field (about 10 V) was applied to the system and the cell was polarized at high current density, the anionic concentration near the positive electrode decreased to zero, and the charge neutrality in its vicinity was violated. Therefore, a positive space charge area and a huge local electric field appeared, which initiated the dendrite growth. It was further indicated that the initiation time corresponded to the building up of the space charge, and the velocity of the dendrite propagation equaled the velocity of the anions.

In 1998, Brissot et al. [49] published their studies on the Li deposition in Li metal secondary batteries with an extremely high current density in the framework of the Chazalviel model. The velocity of the dendrite propagation is a function of the anionic mobility, proportional to the local current density and consistent with the conclusions in Ref. [48]. Moreover, it was observed that the subsequent dendrite growth continued from the electrode surface instead of at the tip of the existing dendrites that grew during previous polarizations, and the dendrites seemed unable to grow beyond a given distance from the negative substrate.

In 1999, Brissot, Rosso and Chazalviel [50] studied three different techniques to measure the concentration maps in Li/polymer cells to validate the correlation between the dendrite growth and the concentration profiles.

From 1999, Rosso, Brissot and Chazalviel [51–53] have made several refinements to improve their previous theory. With the previous homogenous Chazalviel model, a small current was predicted unable to trigger the dendrite formation, which was not coincided with later experimental observations [54]. To solve this contradiction, they supplemented the theory with the consideration of surface non-uniformity, which should be integrated into the Chazalviel model, since the un-uniform microstructure of the electrode surface could trigger the variations of local current density and initiate the dendrite at some locations.

Besides the above three types of models to simulate dendrite initiation and propagation, Yamaki [55] established the correlation between the dynamics of interfacial pressure and the surface tension of two fluids by a fluid dynamic mathematical model, and obtained three types of deposition shapes depending on the calculation of surface tension and internal pressure. It concluded that the Li protrusions grew from the base and were deposited as particles on the surface when the surface tension was large enough to deform the Li whiskers.

The surface-tension model shows substantial establishment on the mechanistic description of the initiation and propagation of the dendrite, while the Brownian statistical simulation model is more effective in the study of dendrite morphology evolution. Unlike the diffusion-controlled mechanism in the above two models, the Chazalviel model elucidates the electromigration-controlled mechanism of the dendritic onset when a high electric field is applied. However, due to the high voltage and current density involved in the mechanism, the original Chazalviel model is supposed not applicable to the study of secondary Li batteries.

It should be noted that the mechanistic models of dendrite initiation and propagation in this section are not limited to the study of Li deposition in Li metal secondary batteries, but also well suited for other electrodeposition phenomenon, including the study of deposition morphology in Li-ion batteries after the Li has deposited at the interface.

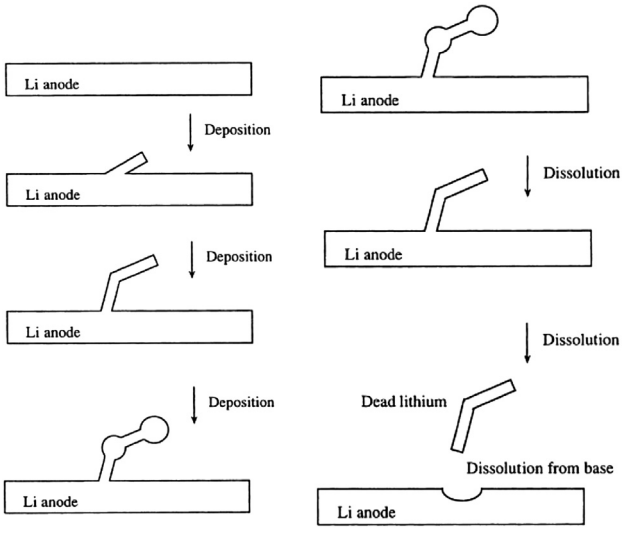

Fig. 5. The Li deposition and dissolution at the Li electrode [55,56] (See Fig. 1 in Ref. [1]).

Table 7
Theories on the preferential location of the next deposition in the early stage of dendrite formation.

Theory	Location preference	Explanation
Barton surface-tension model [32]	The tip of existing protrusions	The enhanced spherical diffusion at the tip of existing protrusions
Brownian simulation model [42–44]	Either the substrate or the tip	The competition mechanism between the ion diffusion and the reductive deposition
Yamaki et al. [55]	The substrate	Not explained
Chazalviel electromigration-limited model [48]	The substrate	The space charge area and huge local electric field in the vicinity of the electrode substrate

Table 8
The impact factors on the morphology of deposited Li.

Category	Factor	
Battery components	Liquid electrolyte	Organic solvent [61,62] Lithium salt [58,60,63,64]
	Gel [65–68]/solid electrolyte [69–73]	
	Electrolyte additives (See Table 9)	
	Current collector [69,74–77]	
Battery working conditions	Current	Charge current density [49,54,62,78–81] Discharge current density [56,82] Pulse charging [46,83]
	Mechanical pressure [57,84,85]	
	Ambient temperature [52,86,87]	
	Stirring [31,60,88]	

3.2. The electrochemical process of Li deposition and the impact of the SEI on the dendrite formation

3.2.1. The electrochemical process of Li deposition

Fig. 5 depicts the basic process of Li deposition and dissolution at the Li electrode. The detailed Li deposition process, including the conditions of dendrite formation, is reported to follow these procedures:

(1) The electrode surface with multiple types of defects, such as pits [56,57], cracks [57], crystalline defects [56], grain boundaries [56] and metal stress lines [57], will result in non-uniform Li deposition under the SEI layer [58,59] and cause mass deformation underneath the SEI layer due to the mechanical stress.
(2) If the SEI layer is elastic and has a good restraint to the underneath structures, or the growth is not continuous at the same spot, the deposited Li will grow as in a mossy or particulate morphology. At the points where the deposition is extensive and the SEI layer is vulnerable, the deposited Li will grow out of the planar surface in the shape of protrusions. In this case, the SEI layer would temporarily break, but still has a good chance to heal again by the ongoing reaction between the electrode and the electrolyte, either at the previously broken spot or wrapped around the newly generated protrusions.
(3) Significant difference has been observed in the theory of Barton–Bockris surface-tension model [32], Brownian simulation model [42–44], Chazalviel electromigration-limited model [48] and the theory of Yamaki [55] on the preferential growth location of the next deposition in the early stage of dendrite formation. The Barton–Bockris model indicated that compared with the linear diffusion at the planar surface of the Li substrate, the enhanced spherical diffusion at the tip of existing protrusions would induce the preferential deposition at the tip. In the Brownian simulation model, a clear explanation has been given in Ref. [46] that the competition between the ion diffusion and the reductive deposition would determine the preferential location of the next deposition statistically, either near the substrate or at the tip of the existing deposition bush. Unlike the above two theories, Yamaki et al. [55] indicated that the Li was still deposited on the substrate instead of at the tip of existing fiber-like protrusions, at least in the early stage of dendrite formation when the surface of the electrode substrate had not been covered with massive protrusions. The theory of Yamaki et al. consisted well with the observation in the study of Chazalviel [48], which concluded that the next growth was also from the electrode surface other than the tip of existing dendrites.
(4) Table 7 compares these different theories on the preferential location of the next deposition in the early stage of dendrite formation. In the late stage, with the protrusion growth at many deposition spots, the electrode surface becomes covered with the deposits and the Li ion transport is hindered. The following deposition in the late stage is more likely to happen on the tips or kinks of the existing protrusions, which helps to shape the Li protrusions like mushrooms [55,56] or dendrites. Although not articulated in each reference, the different theories in Table 7 converge with one another on the preferential location of the next deposition when the process has come to the late stage of dendrite formation.

3.2.2. The impact of the SEI layer on dendrite formation

The morphology of deposited Li could be categorized into three types [56]: mossy [56,57], granular (particle-like) [56–60], and dendritic (or needle-like) [56–60]. It is generally believed that dendritic deposition of Li could easily pierce the separator, causing internal short and thermal runaway of batteries. Furthermore, the dendrite is also prone to the root fracture and produces the dead Li (Fig. 5), resulting in the capacity loss. Therefore, the Li deposition in mossy or granular shapes could achieve higher cycling efficiency and battery safety than the dendritic deposition.

As indicated in the deposition reaction process, the property of the SEI layer has major effects on the morphology of the deposited Li. It was pointed out in Ref. [58], the morphology of the deposited

Table 9
Multiple additives in electrolytes to suppress the dendrite formation.

Mechanism	Electrolyte additives	Effects
Reducing reaction with electrolyte [56]	Saturated hydrocarbons [93] Polyether surfactants [94] Siloxanes [95,96]	In the presence of polyether surfactants, the surface film was stable and with constant thickness due to the coexistence with the polyether [94].
SEI former	Fluoroethylene carbonate (FEC) [59] Vinylene carbonate (VC) [59,75] Polysulfide [97]	Adding FEC into PC solvent [59] could improve the cycle efficiency, since it generated a low-resistance SEI layer and a uniform/closely packed layer of particle-like deposition. Whereas adding VC or ethylene sulfite (ES) would increase the SEI resistance and cause non-uniform deposition as well as efficiency reduction. However, combined with adding Na, adding VC as an SEI former in the electrolyte would lead to significant improvements in cycling efficiency [75].
Forming alloy that disrupts dendrite growth	Metal chloride [56] Sodium (Na) [75]	The added metal chloride would spontaneously form electrochemical alloy with the Li, which made smoother deposition morphologies [56]. Besides, adding a small amount of Na could increase the cycling efficiency [75]. First, the Li and Na co-deposited during charging, and the size mismatch between two metal atoms disrupted the dendrite growth. Second, the metal alloy might form, which was supposed non-dendritic due to the potential criterion.
Mechanical barrier	Fumed Silica [98]	The electrolyte elasticity has been significantly improved by adding fumed silica into the organic liquid electrolytes [98]. A stiff and elastic three-dimensional network was generated in the electrolyte, which provided mechanical support for the system and constrained the development of dendrites. These supporting modules scavenged the impurities in the electrolytes, helping to form smooth and thin SEI layers on the electrode surface.
Enhancing ion diffusivity	Ionic liquid [99–102]	The ionic liquid has attracted attentions due to the advantage of high ion diffusivity. Adding 1-ethyl-3-methylimidazolium bis-(trifluoromethane-sulfonyl) azanide (EMIM-TFSA) into the electrolyte composed of PC/EC and $LiPF_6$ [99] suppressed Li dendrites efficiently. The ionic liquid electrolyte with Zwitter ionic compounds [100–102] could increase the diffusivity of the Li ion and result in a 100% increase of the rate capability. Nuclear magnetic resonance (NMR) spectroscopy, X-ray photoelectron spectroscopy (XPS) and EIS were used to examine the SEI layer: The resistance of the SEI was reduced by 50%, and fewer decomposition products of electrolyte were detected.
/(Impurities introduced by air exposure)	H_2O [58,103] CO_2 [58,103] N_2, Ar, O_2 [103]	H_2O and CO_2 [58,103]: Increasing CO_2 content in PC solution would help to improve the cycle efficiency and reduce the interfacial impedance. Whereas increasing the content of H_2O would benefit the cycling efficiency in the short term, but increase the interfacial impedance in the long-term cycling. The impacts of N_2, Ar and O_2 were also discussed in Ref. [103].

Li was mainly dependent on the 'secondary current distribution' readjusted by the chemical composition and physical microstructure of the SEI layer, rather than the initially-prepared microstructure of the electrode surface before immersed into electrolyte.

The ideal characteristics of the SEI layer have been suggested as follows:

(1) Uniform (with fewer defects). The uniform texture of the SEI layer could generate uniform deposition, which reduces the mechanical stress underneath the layer and protects the intactness of the layer.
(2) Elastic. The volume change during Li deposition and dissolution process in Li electrodes is substantial compared with that during Li intercalation and deintercalation in graphite anodes, which requires the SEI layer to be soft, elastic, and self-healing [59]. An elastic SEI layer could help to restrain the deposited Li growing in the heights (outwards) and encourage the deposition morphology to be particulate or moss-like, instead of in the shape of dendrites.
(3) Low resistance [59]. The SEI layer with lower resistance could facilitate the passing through of Li ions. In particular, when the electrode surface has been partially covered with protrusions, the lower resistance of the SEI layer would increase the probability of Li deposition on the substrate [56], suppress the deposition on the tips or kinks of existing protrusions, and obstruct the formation of dendrites.

It is worth noting that, although the importance of the SEI layer has been emphasized in the literature, focusing on the improvement measures of the SEI layer quality; sometimes, even as the dominating factor, the role of the SEI layer was rarely included and discussed in the mechanistic models in Section 3.1. A gap between the practical measures and the mechanistic cognition has been observed on the role of the SEI layer in determining the Li deposition morphology. More details on the role of the SEI layer will be discussed in Section 4.2.

3.3. The impact factors on the morphology of the deposited Li

In this section, the most important impact factors on the deposition morphology, which have been extensively discussed in the literature, are reviewed following the framework described in Table 8.

3.3.1. Battery components

(1) The liquid electrolyte composed of organic solvents and lithium salts

The composition and concentration of organic solvents: The cycling efficiency of Li metal secondary batteries was proved to be closely related with the composition and concentration of organic solvents. In Ref. [61], the different effects of multiple organic solvents in the electrolyte of Li metal secondary batteries, including ethylene carbonate (EC), propylene carbonate (PC), dimethyl carbonate (DMC), diethyl carbonate (DEC) and ether, were studied. In Ref. [62], it has been shown that the onset of dendrites had been delayed when reducing the PC solvent content in the PC/Li bis-(trifluoromethanesulfonyl) imide (LiTFSI) electrolyte system.

The composition and concentration of lithium salts: It was reported [60] that the lithium salt $LiPF_6$ contributed to the generation of uniform and smooth SEI layers as well as deposited Li since the presence of HF in the electrolyte would react with the deposited Li to produce LiF in the SEI composition, helping to shape the deposition into more favorable morphologies.

This observation has been further supported by the work in Ref. [63], which showed that, compared with $LiClO_4$, $LiPF_6$ in the electrolyte generated fewer types of layer-forming salts and smoother Li deposition, inhibiting the dendrite occurrence and extending the battery life. Subsequently, the work in Ref. [58] suggested that $LiAsF_6$ could achieve better interfacial smoothness compared with the first two lithium salts of $LiPF_6$ and $LiClO_4$.

Furthermore, enhancing the lithium salt concentration could reduce the thickness and the resistance of the SEI layer, thus suppress the dendrite formation and improve the battery cycling efficiency [64]. In the PC/$LiN(SO_2C_2F_5)_2$ electrolyte system, when increasing the concentration of the lithium salt from 1.28 to 3.27 mol kg^{-1}, the SEI layer thickness was reduced from 35 nm to 20 nm, and the cycling number before the efficiency declined to 80% has been increased from 10 to more than 50.

(2) The gel/solid electrolyte

Aurbach et al. carried out a series of studies [1,58,63,89–92] to improve the performance of Li electrodes in the liquid electrolyte, including the modification to the electrode material and to the species of lithium salts, organic solvents and additives. After these studies, it was found that it was impossible to modify the morphology of electrode surfaces to be dendrite-free when the applied charging rate was high. And the feasible charging rate should be extremely small to obtain satisfactory surface morphologies, e.g., 0.1 C. This limitation has restrained the application of secondary Li metal batteries on portable electronics or electric vehicles. Therefore, they concluded that Li metal secondary batteries with liquid electrolyte composed of organic solvents and lithium salts could be substituted by batteries with gel or all-solid electrolytes to solve the limitation of dendrite propensity under applicable charging rates [1,91].

It was reported that [65–68], these types of 'stiff and elastic' gel-type electrolytes, which were produced by soaking polymer materials in liquid electrolytes with organic solutions and lithium salts, could suppress the formation of Li dendrites and generate smooth and uniform deposition. This inhibition effect was attributed to the rigidity of the gel, which imposed strong mechanical restraints to the growth of dendrites.

Besides the Li batteries with gel-type polymer electrolytes, thin-film solid Li batteries (TFB) using all-solid inorganic electrolytes [69–73] also achieved high safety and cycling efficiency due to the advantages on non-flammability and dendrite inhibition of this TFB system.

(3) Electrolyte additives

Table 9 summarizes the multiple additives in electrolytes, which could suppress the dendrite formation, in different categories according to the mechanisms.

(4) The current collector

Alloying reactions as a strategy to avoid Li dendrite formation has been pursued for decades as reported in the literature, which deserves attention. Application of graphite as the negative electrode is born from such a strategy, which has led the rapid development of Li-ion batteries. In contrast to the Li intercalation in graphite, alloying of Li with some metals such as Al and Sn or semiconductors such as Si involves displacement reactions that come with more severe mechanical stability issues with their volume changes.

The work reported in Ref. [69] showed that a thin platinum layer, with less than 10 nm in thickness, was inserted between the solid electrolyte and the copper film current collector, and this layer alloyed with Li at the interface. It was observed using the electron microscopy that the platinum dispersed in the plated lithium at the interface, and it was deduced that more Li plating sites between the electrolyte and the current collector were generated, resulting in the reduction of the overvoltage of the lithium plating stripping reaction and a more uniform and smooth surface morphology.

In Ref. [74], an Al sheet of 0.2 mm thick was used as the negative electrodes for the Li electrodeposition. It was observed that the Li has reacted with Al and caused the formation of Al–Li alloy. The result indicated that the cell achieved good cycling efficiency by using Al instead of Li as the substrate. Similarly, a Li–Al alloy was formed at the interface of the Al substrate and the electrolyte composed of PC solution and $LiClO_4$ [77], and it was also indicated that the battery with this anode had achieved excellent cycling efficiency probably due to the preferred microstructure of the Al substrate.

Spatially anisotropic but heterogeneous three-dimensional current collectors, prepared by depositing a thin SiO_2 layer onto a carbon-fiber paper, have been introduced in Ref. [76]. Instead of allowing Li deposition at the electrolyte interface, the new type of current collector accommodated the Li deposition inside the spacious voids, which was confirmed to be dendrite-free by ex-situ SEM observation even at high current densities.

However, it is worth noting that the alloying of Li with other metals may cause large volume change and hamper its mechanical stability, resulting in a side effect of reducing its cycling efficiency instead.

3.3.2. Battery working conditions

(1) The current density

The charge current density:

In 1998 , Brissot et al. [49] predicted that the growth velocity of the dendrite is proportional to the local current density. In 1998 and 1999, Orisin et al. [78,79] reported that the morphology of the deposited Li had an apparent correlation with the current density in Li batteries. It was shown that a low current density led to a mossy deposition after the first charge, whereas the deposition became more dendritic at higher current densities. In 2002, by means of a SEM equipped with a transfer system which could prevent the sample exposure in the air, it has been observed by the same group [80] that if the local current density was enlarged from 0.22 to 0.50 mA cm^{-2}, the shape of the deposited Li changed from moss-like to needle-like, which was in good agreement with their previous observations.

In 2006, Rosso et al. reported the results of the fuse effect time t_{fe} [54], which reflected the charging time elapsed before the battery short due to the development of one or several dendrites. It has been observed that the fuse effect time roughly varied with the applied current density J in the following correlation:

$$t_{fe} \sim J^{-2} \tag{6}$$

The same correlation has also been observed in 2008 [62]. With the decrease of the current density, the onset of the first dendrite was delayed in proportion with the Tafel resistance, which was the local slope of the polarization curve.

The impact of current density on dendrite formation in the Li powder anode was studied in 2008 [81]. In this type of system, it was reported that the formation of dendrites was influenced by the current density, but mostly determined by the 'total amount of discharge', which represented the degree of dissolution (or the state of charge) of the Li powder.

The discharge current density:

Besides the charge current, the discharge current also has considerable impacts on the deposition morphology and battery cycling efficiency. It was indicated in Ref. [82] that, the cycle life of battery decreased with the increase of charge current density, but with the decrease of discharge current density. This impact was attributed to the inhibition of the dead Li creation under high discharge current rates [56]. Furthermore, high rates could lead to the recombination of the isolated Li (dead Li), resulting in the increase of cycle efficiency.

The pulse charging:

It was reported that pulse charging could alter the surface morphology of electrodeposition advantageously in multiple types of metals and alloys [83]. Based on the simulation results by the Brownian simulation model in Section 3.1.2, the work reported in Ref. [46] indicated that 'shorter and more widely spaced' charging pulses could suppress the dendrite formation and improve the deposition morphology most effectively.

(2) The mechanical pressure

The mechanical pressure was shown to have considerable impacts on the Li deposition morphology, the dendrite propensity and the battery cycling efficiency [84].

An 'isolation prevention' strategy was proposed by Hirai et al. [85] based on the correlation of the cycling efficiency and the mechanical pressure. The Li surface morphology after the first charging was observed with and without stack pressure. SEM results indicated that dense and uniform depositions could be generated under a stack pressure. The work suggested that Li deposited under high pressure was not easily isolated from the substrate during stripping due to the dense structure, which enhanced the cycling efficiency.

A 'dendrite-growth confining' strategy was proposed in Ref. [57] to utilize the impact of pressure on dendrite suppression. It was suggested that the development of dendrites was unavoidable owing to the defects existing in the intrinsic microstructure of Li, but by applying a compressive load on the internal cell components, the dendrite could be confined in the vicinity of the negative electrode surface and the development in its length direction could be inhibited. The suppression of dendrites had contributed significantly to the battery cycling performance. It was shown in Fig. 6 that with the increase of pressure from 0.7 kg cm^{-2} to 7 kg cm^{-2}, the cycling efficiency had been raised from 50% to 80% at the initial cycle, and kept above 80% instead of decreasing sharply down to 20% after 10 cycles.

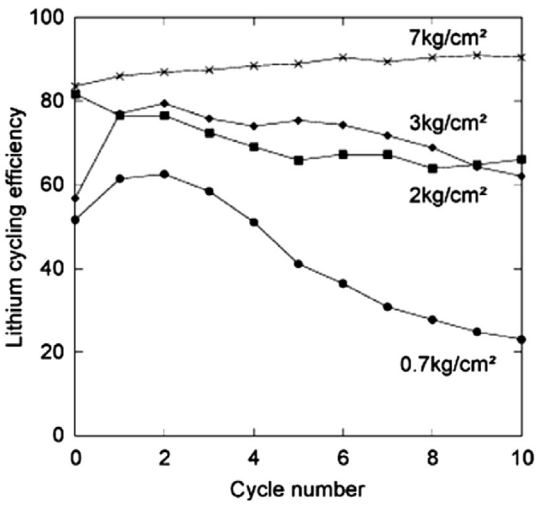

Fig. 6. The cycling efficiency under different pressures [57].

(3) The ambient temperature

The Li deposition on a nickel substrate in 1 M lithium bis-(perfluoroethylsulfonyl) imide (LiBETI) dissolved in the PC solution was studied to reveal the correlation between the cycling efficiency and the ambient temperature by Mogi et al. [86]. They proposed that the reductive decomposition of electrolyte was much faster at elevated temperatures such as 80 °C, and the SEI layer rapidly formed in the initial depositions. Meanwhile, the defects on the SEI surface, like cracks, could be repaired in a short time. This rapid-forming and self-repairing SEI layer enabled the underneath deposition to grow into a flat, uniform and smooth morphology, thereby inhibited the dendrite propagation and improved the cycling efficiency. Compared with room temperature, the cycling efficiency at 80 °C has been significantly increased. At room temperature, the initial efficiency was 60% ~ 70%, and rapidly dropped to 20% after 30 cycles, whereas at 80 °C the efficiency kept above 70% during the first 30 cycles.

In contrast, Park et al. [87] observed that a faster dendrite growth occurred at higher ambient temperatures in a similar magnitude of current density with the above case in Ref. [86] (1 and 0.5 mA cm^{-2} for the two cases, respectively). The elapsed time until a short occurred due to the dendrite growth reaching the counter electrode [52] was observed at −5 °C, 15 °C, and 35 °C in a Li/Li coin cell in electrolyte of 1 M $LiPF_6$ and 1:1:1 EC/DMC/EMC (ethyl methyl carbonate) [87]. 1 mm Teflon was used as the separator, which was extremely thick to enlarge the cell resistance and extend the 'elapsed time' for better resolution. A longer 'elapsed time' and a slower dendrite growth were observed at lower temperatures.

Seemingly, contradictive results have been demonstrated in the above two cases reported in Refs. [86,87]. These contradicting effects caused by temperature on the dendrite formation could be attributed to the bifurcate effect of temperature on the SEI quality and the dendrite growth rate. Higher temperatures result in a speedier formation of the SEI layer with a more uniform and smoother morphology than those at lower temperatures, which is beneficial to the dendrite suppression. On the other hand, higher temperatures could also promote the ion diffusion around the deposition locations and accelerate the growth of the existing dendrites, which inclines to trigger the battery short in a shorter time. The dominating factors between the two opposing effects may have altered the results in the studies of the above two cases, due to the differences in the battery system, electrolyte composition and temperature-induced kinetic variations.

(4) Stirring

As indicated in Section 3.3.1 (1), the presence of HF in the electrolyte with $LiPF_6$ could shape the deposited Li into a favorable morphology under the SEI layer. By applying a rotating disk electrode [60], the transmission of the HF has been increased and its effect on the dendrite inhibition improved. Similarly, a rotating disk electrode was also applied in the work reported in Ref. [31] to study the dendrite formation on the Li and the Al–Li electrode surface. It was found that the rotating electrode could relax the concentration

gradient in the electrolyte and exclude the impact of the gradient on the measured potential. In Ref. [88] it was reported that the Li dendrite was found at 0.5 mA cm^{-2} under static conditions, whereas uniformly distributed hemispherical particles of the deposited Li were detected at the current density as high as 2.0 mA cm^{-2} under dynamic conditions created by magnetic stirring.

3.4. The observation methods of Li deposition

3.4.1. The imaging methods by the optical microscopy, SEM and atomic force microscope (AFM)

Arakawa et al. [82] observed in situ Li deposition in liquid electrolyte using the optical microscopy in 1993. Osaka et al. [104] evaluated the electrodeposited Li on nickel substrate by the optical microscopy in two types of liquid solutions to investigate the correlation between the surface morphology and the resistance distribution in 1993 and studied the Li deposition process in liquid, gel and solid electrolyte [68]. Brissot et al. published a series of papers [49–51,54] to study Li deposition in poly-(ethyleneoxide)/Li-salt electrolytes using a charge-coupled device (CCD) camera fit on an optical microscope in 1998–2006.

From 1990s, SEM and AFM [63,105,106] have been extensively used for in situ and *ex situ* studies of the behavior of Li deposition in many electrolyte systems and achieved much better resolutions than optical imaging methods. To avoid the possible contamination of the sample or the secondary reaction with atmospheric components, special attachments have been developed [78–80] to provide vacuum environment in the sample transfer process.

3.4.2. NMR

Although the optical microscopy, SEM and AFM could visually reveal the morphology of the Li deposition, these methods are not suited for quantitative studies in dynamic conditions. In Ref. [107] in situ NMR spectroscopy was used in the observations of Li deposition, which provided time-resolved quantitative information about the deposition on Li metal electrodes. The work reported in Ref. [99] showed that the NMR spectroscopy could reveal the 'skin-depth' of the electrodes with a penetration depth of 14.7 μm to monitor the chemical changes in this range of depth. The presence of the 'two Li resonance peaks' in the NMR spectra [107] was attributed to different surface structures on the Li electrode during charging. The first resonance peak, approximately at the same position of the original resonance peak in the spectra of a fresh cell, was assigned to the remaining initial Li surface. The second resonance peak was explained by the growth of new Li deposition as dendrites on the surface. Recently, Chandrashekar et al. revealed the location of microstructural Li as a result of charging using the magnetic resonance imaging (MRI) technique with a Li metal symmetric cell [3]. This approach provides quantitative information of the compositions, as well as high spatial resolution, and could be readily applied to explore the formation of dendrites under different electrochemical conditions (charging/discharging rates, different electrolyte salts, additives or solvents, etc.) to help in improving the design of batteries.

3.4.3. EIS

It has been observed by EIS in Ref. [99] that in a $Li/Li_4Ti_5O_{12}$ battery in $LiPF_6$ and EC/DMC electrolyte, the higher-frequency resistance related to the SEI layer decreased with time rapidly, which was caused by the SEI damage due to the dendrite formation.

Osaka et al. used a similar method to study the electrodeposited Li on nickel substrate [104]. The result of EIS was compared with the imaging from the optical microscopy to show the correlation between the surface morphology and the impedance distribution. It was suggested that the impedance obtained from the higher frequency region in the EIS represents the morphological state of the deposition structure. In Ref. [88] the cell impedance evolution was measured from two symmetric Li cells with polymer electrolyte, whereas in each symmetric cell the two electrodes were made of electrodeposited Li films and commercial Li foils, respectively. The EIS results showed that the interfacial impedance of both cells increased during cycle aging. Furthermore, the interfacial impedance of the cell with electrodeposited Li films as the electrodes was relatively small and the cell reached equilibrium more quickly.

The cell impedance evolution of Li polymer cells was also measured by EIS in the work of Ref. [79]. Similarly, an increase in the interfacial impedance with the ongoing cycle aging has been observed.

In addition, the characterization methods to detect the material composition, such as XRD or XPS, were used in the study of Li deposition. Although the composition of the surface has certain impacts on the morphology, the morphology characterization technologies such as SEM and AFM are more effective to observe the detrimental formation of dendrites directly. Therefore, the composition analysis and characterization methods are less emphasized in the scope of this paper.

4. Discussions

4.1. Criteria for Li deposition

The concentration and potential criteria: The two criteria of Li deposition in Li-ion battery have been summarized in Table 2. The first depicts that Li would be deposited if the Li ion concentration at the interface exceeds the saturation [4]. The second criterion states that Li would be deposited if the potential across the interface falls below that of Li/Li^+. Although not verified in the work of Ref. [4], the potential criterion at the interface was expected to satisfy the concentration one simultaneously. In this case, the two criteria become equivalent. However, it is possible that Li could deposit due to overpotential well before its concentration reaches local saturation. Therefore, the potential criterion is more critical.

The effect of substrate on the open circuit potential of the Li deposition reaction (U_o): For the Li deposition on bulk Li metal, U_o is zero at a specific temperature. Therefore, in most cases the criterion $\eta^{+}_{Li/Li} < 0$ was actually used as to denote $\phi_n < 0$ in the literature (see Eq. (1)). However, the Li deposition on the surface other than Li metal shall cause $U_o > 0$. In this case, although the criterion $\eta^{+}_{Li/Li} < 0$ is still held, the criterion used in practice should be changed to $\phi_n < U_o$ instead of $\phi_n < 0$, and the value of U_o should be redetermined. It was observed that a significant amount of Li deposited on the graphite when the graphite was charged and held at 5 mV vs. Li/Li^+ [10]. Although it was observed under −5 °C, this phenomenon should be largely attributed to the change of substrate material.

In addition, the particle size may also play a role in the initial stage of deposition due to the high surface tension of initial Li nucleation. Other surface conditions, including local concentrations of disorders, microstructural defects and the degree of graphitization are all expected to influence the value of U_o.

The effect of subsequent reactions on the deposition criteria: The potential criterion of the reversible Li deposition has been set as $\eta_{Li/Li^+} < 0$. However, the deposited Li could pierce the SEI layer and react with the electrolyte to form insoluble byproducts, which makes the Li deposition semi-reversible. These subsequent reactions could shift the critical potential of Li deposition into a positive range. Therefore, instead of a theoretically distinct value of '0 V', the Li deposition reaction may occur within a positive interval

of potentials, and the extent of this interval depends on the species and intensity of the following reactions.

4.2. The role of the SEI layer in the dendrite models of Li metal secondary batteries

As indicated in Section 3.2, the role of the SEI layer was rarely considered in the dendrite models. From a survey of the literature, although the result in Ref. [58] has contended that the rate-determining step of all these procedures is only Li ion migration through the surface film, most reports in the literature directly proceed to the modification of electrolyte composition to refine the conditions related to the SEI layer formation, without justifying the importance of the SEI layer in the deposition process.

To investigate the role of the SEI layer plays in the Li deposition, the stepwise sequential processes (such as adsorption and desolvation) for a Li ion to go through from electrolyte to deposition underneath the SEI layer should be considered. Among these steps, the importance of the transport through the SEI layer should be elucidated in comparison with other processes. Along with a better understanding of the sequential processes such as ion migration, reduction and their respective impacts on the deposition morphology, the proposed measures to refine the conditions related to the SEI layer formation will be well targeted and more efficient in dendrite suppression.

4.3. The pre-heating measure to prevent Li deposition in Li-ion batteries at low temperatures

The pre-heating measure prior to the commencement of charging at low temperatures should be evaluated in depth before it could be adopted in real applications in BTMS. A common approach is to add an external heater inside the battery pack housing, which has been adopted in several BTMS of electric vehicles. As suggested by Pesaran et al. [29], the typical problems of external heating are mainly related to its low heating efficiency and the presence of a temperature gradient inside the battery. To solve the problems of the external heating, an internal heating method using high-frequency AC self-heating has been introduced in Section 2.4 and has achieved a high heating rate in a relatively short time.

For further optimization, the detailed parameter setting of this self-heating method should be characterized. The suitable range of the frequency band and AC amplitude should be studied by comparative experiments. In addition, the effect of this heating method on battery degradation should be evaluated thoroughly. The battery DC resistance or AC impedance spectroscopy should be monitored along with the thermal cycling aging.

5. Conclusions

For Li-ion batteries, the risk of battery short induced by the Li deposition on the graphite anode has been the main concern of fast charging (e.g., fully charged in less than 1 h) and low-temperature charging (e.g., $<0\ ^{\circ}C$). The deposition criteria and models of Li-ion batteries reviewed in this paper could help in predicting the threshold of deposition occurrence and evaluating effective measures to prevent the Li deposition during charging. The charging protocols in practical use, which simulate an ideal charging according to the theoretical models, are reviewed. These efforts should assist improving commercial charging methodology.

For Li metal secondary batteries, the electrodeposition of Li on Li electrodes is a necessary step to complete the electrochemical reaction. The morphology control of the deposited Li is key to success, whereas shaping the Li deposition into smooth and harmless features is vital for such control. In the theoretical aspects, several models have been presented to elucidate the mechanism of dendrite initiation as well as to simulate its growth processes. In the aspect of application, numerous attempts have been made to refine different components in the battery system to assist favorable Li deposition. In particular, modifications to the SEI formation are most intensively studied. The volume change of active materials in the Li electrode of Li metal secondary batteries is significantly higher than that in the graphite anode of Li-ion batteries, which implies that the SEI layer on the Li electrode is highly required to exhibit good elasticity in order to inhibit the Li dendrite growth. Adding additives to the electrolyte could produce a better SEI layer with required composition and morphology and provide better mechanical support or higher ion diffusivity in the electrolyte system. In addition, the control of battery working conditions, such as current density, pressure and temperature, could also produce favorable effects on the deposition morphology.

The survey of the literature leads to some important lessons and inspirations on further exploration to better control of Li deposition. The universality of two criteria for Li deposition is discussed first. The effects of the substrate and its properties and the subsequent reactions stipulated by the potential criterion should be considered. The sequential steps in the Li deposition that involve ion migration and reduction and their respective impacts on the deposition morphology should be characterized to understand the importance of the SEI layer in determining the deposition morphology. Finally, the pre-heating measure before the commencement of charging at low temperatures should be investigated in depth to refine its potential for adoption in real BTMS applications. Possible solutions include high-frequency AC self-heating. The effectiveness and drawbacks of this method should be quantitatively evaluated, and the frequency band and current amplitude of the AC wave pattern should be optimized.

Acknowledgments

This work is supported by the National Natural Science Foundation of China under grant number 51207080, the China Postdoctoral Science Foundation under grant number 2012M510436, and the Independent Research Programs of Tsinghua University under subject number 2011Z01004.

References

[1] D. Aurbach, E. Zinigrad, Y. Cohen, H. Teller, Solid State Ionics 148 (2002) 405–416.
[2] H. Honbo, K. Takei, Y. Ishii, T. Nishida, J. Power Sources 189 (2009) 337–343.
[3] S. Chandrashekar, N.M. Trease, H.J. Chang, L.-S. Du, C.P. Grey, A. Jerschow, Nat. Mater. 11 (2012) 311–316.
[4] B.K. Purushothaman, U. Landau, J. Electrochem. Soc. 153 (2006) A533–A542.
[5] P. Arora, M. Doyle, R.E. White, J. Electrochem. Soc. 146 (1999) 3543–3553.
[6] M. Doyle, T.F. Fuller, J. Newman, J. Electrochem. Soc. 140 (1993) 1526–1533.
[7] M. Tang, P. Albertus, J. Newman, J. Electrochem. Soc. 156 (2009) A390–A399.
[8] R.D. Perkins, A.V. Randll, X. Zhang, G.L. Plett, J. Power Sources 209 (2012) 318–325.
[9] G. Park, N. Gunawardhana, H. Nakamura, Y.S. Lee, M. Yoshio, J. Power Sources 199 (2012) 293–299.
[10] G. Park, N. Gunawardhana, H. Nakamura, Y.S. Lee, M. Yoshio, J. Power Sources 196 (2011) 9820–9824.
[11] J.A. Mas, US Patent 3,683,256, August 8, 1972.
[12] J.A. Mas, US Patent 3,732,481, May 8, 1973.
[13] J.A. Mas, US Patent 3,816,806, June 11, 1974.
[14] S.S. Zhang, K. Xu, T.R. Jow, J. Power Sources 160 (2006) 1349–1354.
[15] L. Li, X. Tang, Y. Qu, H. Liu, J. Cent, South Univ. Technol. 18 (2011) 319–322.
[16] C. Park, Z. Zhang, Z. Xu, A. Kakirda, K. Kang, C. Chai, G. Au, L. Cristo, J. Power Sources 165 (2007) 892–896.
[17] Y. Liu, J. Teng, Y. Lin, IEEE Trans. Ind. Electron. 52 (2005) 1328–1336.
[18] S.K. Chung, A.A. Andriiko, A.P. Mon'ko, S.H. Lee, J. Power Sources 79 (1999) 205–211.
[19] G. Sikha, P. Ramadass, B.S. Haran, R.E. White, B.N. Popov, J. Power Sources 122 (2003) 67–76.

[20] P.H.L. Notten, J.H.G. Veld, J.R.G. Beek, J. Power Sources 145 (2005) 89–94.
[21] J. Li, E. Murphy, J. Winnick, P.A. Kohl, J. Power Sources 102 (2001) 302–309.
[22] X.W. Zhao, G.Y. Zhang, L. Yang, J.X. Qiang, Z.Q. Chen, J. Therm. Anal. Calorim. 104 (2011) 561–567.
[23] L. Chen, S. Wu, D. Shieh, T. Chen, IEEE Trans. Ind. Electron. 60 (2013) 88–97.
[24] S.J. Huang, B.G. Huang, F.S. Pai, IEEE Trans. Power Electron. 28 (2013) 1555–1562.
[25] T.A. Stuart, A. Hande, J. Power Sources 129 (2004) 368–378.
[26] A. Hande, T.A. Stuart, IEEE Power Electron. Transp. (2002) 119–124.
[27] Hande, in: Proceedings of the 2004 IEEE Workshop on Computers in Power Electronics, 2004, pp. 215–222.
[28] Ashtiani, T. Stuart, US Patent 6,259,229, July 10, 2001.
[29] A.A. Pesaran, A. Vlahinos, T.A. Stuart, in: The 6th ASME-JSME Thermal Engineering Conference, Hawaii Island, Hawaii, March 17–20, 2003.
[30] http://gm-volt.com/2010/12/09/the-chevrolet-volt-coolingheating-systems-explained/.
[31] Epelboin, M. Froment, M. Garreau, J. Thevenin, D. Warin, J. Electrochem. Soc. 127 (1980) 2100–2104.
[32] J.L. Barton, J.O. Bockris, Proc. R. Soc. Lond. A 268 (1962) 485–505.
[33] J.W. Diggle, A.R. Despic, J.O.'M. Borckis, J. Electrochem. Soc. 112 (1969) 1503–1514.
[34] C. Monroe, J. Newman, J. Electrochem. Soc. 150 (2003) A1377–A1384.
[35] C. Monroe, J. Newman, J. Electrochem. Soc. 151 (2004) A880–A886.
[36] W.W. Mullins, R.F. Sekerka, J. Appl. Phys. 34 (1963) 323–329.
[37] W.W. Mullins, R.F. Sekerka, J. Appl. Phys. 35 (1964) 444–451.
[38] R. Aogaki, T. Makino, Electrochim. Acta 26 (1981) 1509–1517.
[39] T.A. Witten, L.M. Sander, Phys. Rev. Lett. 47 (1981) 1400–1403.
[40] P. Meakin, Phys. Rev. A 27 (1983) 2616–2623.
[41] P. Meakin, Phys. Rev. B 30 (1984) 4030–4037.
[42] R.F. Voss, M. Tomkiewicz, J. Electrochem. Soc. 132 (1985) 371–375.
[43] G. Nagy, Y. Sugimoto, G. Denuault, J. Electroanal. Chem. 433 (1997) 167–173.
[44] R.V. Magan, R. Sureshkumar, B. Lin, J. Phys. Chem. B 107 (2003) 10513–10520.
[45] R.V. Magan, R. Sureshkumar, Nanotechnology 16 (2005) S545–S553.
[46] M.Z. Mayers, J.W. Kaminski, T.F. Miller, J. Phys. Chem. C. 116 (2012) 26214–26221.
[47] W.G. Huang, D.B. Hibbert, Phys. Rev. E 53 (1996) 727–730.
[48] J.-N. Chazalviel, Phys. Rev. A 42 (1990) 7355–7367.
[49] C. Brissot, M. Rosso, J.-N. Chazalviel, P. Baudry, S. Lascaud, Electrochim. Acta 43 (1998) 1569–1574.
[50] C. Brissot, M. Rosso, J.-N. Chazalviel, J. Electrochem. Soc. 146 (1999) 4393–4400.
[51] C. Brissot, M. Rosso, J.-N. Chazalviel, S. Lascaud, J. Power Sources 81 (1999) 925–929.
[52] M. Rosso, T. Gobron, C. Brissot, J.-N. Chazalviel, S. Lascaud, J. Power Sources 97–98 (2001) 804–806.
[53] M. Rosso, E. Chassaing, J.-N. Chazalviel, T. Gobron, Electrochim. Acta 47 (2002) 1267–1273.
[54] M. Rosso, C. Brissot, A. Teyssot, M. Dollé, L. Sannier, J.-M. Tarascon, R. Bouchet, S. Lascaud, Electrochim. Acta 51 (2006) 5334–5340.
[55] J. Yamaki, S. Tobishima, K. Hayashi, K. Saito, Y. Nemoto, M. Arakawa, J. Power Sources 74 (1998) 219–227.
[56] J. Yamaki, S. Tobishima, Rechargeable lithium anodes, in: C. Daniel, J.O. Besenhard (Eds.), Handbook of Battery Materials, second ed., Wiley-VCH, Weinheim, Germany, 2011. Chapter. 13.
[57] L. Gireaud, S. Grugeon, S. Laruelle, B. Yrieix, J.-M. Tarascon, Electrochem. Commun. 8 (2006) 1639–1649.
[58] D. Aurbach, Y. Cohen, J. Electrochem. Soc. 144 (1997) 3355–3360.
[59] Ryo Mogi, M. Inaba, S.-K. Jeong, Y. Iriyama, T. Abe, Z. Ogumi, J. Electrochem. Soc. 149 (2002) A1578–A1583.
[60] N. Langenhuizen, J. Electrochem. Soc. 145 (1998) 3094–3099.
[61] K. Hayashi, Y. Nemoto, S. Tobishima, J. Yamaki, Electrochim. Acta 44 (1999) 2337–2344.
[62] O. Crowther, A.C. West, J. Electrochem. Soc. 155 (2008) A806–A811.
[63] D. Aurbach, Y. Cohen, J. Electrochem. Soc. 143 (1996) 3525–3532.
[64] S.-K. Jeong, H.-Y. Seo, D.-H. Kim, H.-K. Han, J.-G. Kim, Y.B. Lee, Y. Iriyama, T. Abe, Z. Ogumi, Electrochem. Commun. 10 (2008) 635–638.
[65] T. Tatsuma, M. Taguchi, M. Iwaku, T. Sotomura, N. Oyama, J. Electroanal. Chem. 472 (1999) 142–146.
[66] T. Tatsuma, M. Taguchi, N. Oyama, Electrochim. Acta 46 (2001) 1201–1205.
[67] T. Matsui, K. Takeyama, Electrochim. Acta 40 (1995) 2165–2169.
[68] T. Osaka, T. Homma, T. Momma, H. Yarimizu, J. Electroanal. Chem. 421 (1997) 153–156.
[69] K. Okita, K. Ikeda, H. Sano, Y. Iriyama, H. Sakaebe, J. Power Sources 196 (2011) 2135–2142.
[70] K. Kanehori, K. Matsumoto, K. Miyauchi, T. Kudo, Solid State Ionics 9–10 (1983) 1445–1448.
[71] S.D. Jones, J.R. Akridge, F.K. Shokouhi, Solid State Ionics 69 (1994) 357–368.
[72] J.B. Bates, N.J. Dudney, B. Neudecker, A. Ueda, C.D. Evans, Solid State Ionics 135 (2000) 33–45.
[73] Y. Iriyama, K. Nishimoto, C. Yada, T. Abe, Z. Ogumi, K. Kikuchi, J. Electrochem. Soc. 153 (2006) A821–A825.
[74] P. Suresh, A.K. Shukla, S.A. Shivashankar, N. Munichandraiah, J. Power Sources 132 (2004) 166–171.
[75] J.K. Stark, Y. Ding, P.A. Kohl, J. Electrochem. Soc. 158 (2011) A1100–A1105.
[76] X. Ji, D.-Y. Liu, D.G. Prendiville, Y. Zhang, X. Liu, G.D. Stucky, Nano Today 7 (2002) 10–20.
[77] N. Kumagai, Y. Kikuchi, K. Tanno, J. Appl. Electrochem. 22 (1992) 620–627.
[78] F. Orsini, A. du Pasquier, B. Beaudouin, J.M. Tarascon, M. Trentin, N. Langenhuizen, E. de Beer, P. Notten, J. Power Sources 81 (1999) 918–921.
[79] F. Orsini, A. Du Pasquier, B. Beaudoin, J.M. Tarascon, M. Trentin, N. Langenhuizen, E. De Beer, P. Notten, J. Power Sources 76 (1998) 19–29.
[80] M. Dollé, L. Sannier, B. Beaudoin, M. Trentin, J.-M. Tarascon, Electrochem. Solid State Lett. 5 (2002) A286–A289.
[81] I.W. Seong, C.H. Hong, B.K. Kim, W.Y. Yoon, J. Power Sources 178 (2008) 769–773.
[82] M. Arakawa, S. Tobishima, Y. Nemoto, M. Ichimura, J. Yamaki, J. Power Sources 43 (1993) 27–35.
[83] M.S. Chandrasekar, M. Pushpavanam, Electrochim. Acta 53 (2008) 3313–3322.
[84] D.P. Wilkinson, H. Blom, K. Brandt, D. Wainwright, J. Power Sources 36 (1991) 517–527.
[85] T. Hirai, I. Yoshimatsu, J. Yamaki, J. Electrochem. Soc. 141 (1994) 611–614.
[86] R. Mogi, M. Inaba, T. Abe, Z. Ogumi, J. Power Sources 97–98 (2001) 265–268.
[87] H.E. Park, C.H. Hong, W.Y. Yoon, J. Power Sources 178 (2008) 765–768.
[88] X. Yang, Z. Wen, X. Zhu, S. Huang, Solid State Ionics 176 (2005) 1051–1055.
[89] D. Aurbach, H. Teller, E. Levi, J. Electrochem. Soc. 149 (2002) A1255–A1266.
[90] D. Aurbach, M. Koltypin, H. Teller, Y.S. Cohen, Phys. Chem. 229 (2006) 197–211.
[91] D. Aurbach, E. Zinigrad, H. Teller, Y. Cohen, G. Salitra, H. Yamin, P. Dan, E. Elster, J. Electrochem. Soc. 149 (2002) A1267–A1277.
[92] D. Aurbach, E. Zinigrad, H. Teller, P. Dan, J. Electrochem. Soc. 147 (2000) 1274–1279.
[93] J.O. Besenhard, J. Gürtler, P. Komenda, A. Paxinos, J. Power Sources 20 (1987) 253–258.
[94] M. Mori, Y. Naruoka, K. Naoi, D. Fauteux, J. Electrochem. Soc. 145 (1998) 2340–2348.
[95] T. Inose, S. Tada, H. Morimoto, S. Tobishima, J. Power Sources 161 (2006) 550–559.
[96] T. Takeuchi, S. Noguchi, H. Morimoto, S. Tobishima, J. Power Sources 195 (2010) 580–587.
[97] S.I. Tobishima, H. Yamamoto, M. Matsuda, Electrochim. Acta 42 (1997) 1019–1029.
[98] X.-W. Zhang, Y. Li, S.A. Khan, P.S. Fedkiw, J. Electrochem. Soc. 151 (2004) A1257–A1263.
[99] N. Schweikert, A. Hofmann, M. Schulz, M. Scheuermann, S.T. Boles, T. Hanemann, H. Hahn, S. Indris, J. Power Sources 228 (2013) 237–243.
[100] N. Byrne, P.C. Howlett, D.R. MacFarlane, M. Forsyth, Adv. Mater. 17 (2005) 2497–2501.
[101] N. Byrne, P.C. Howlett, D.R. MacFarlane, M.E. Smith, A. Howes, A.F. Hollenkamp, T. Bastow, P. Hale, M. Forsyth, J. Power Sources 184 (2008) 288–296.
[102] C. Tiyapiboonchaiya, J.M. Pringle, J. Sun, N. Byrne, P.C. Howlett, D.R. MacFarlane, M. Forsyth, Nat. Mater. 3 (2004) 29–32.
[103] V.R. Koch, J.H. Young, J. Electrochem. Soc. 125 (1978) 1371–1377.
[104] T. Osaka, T. Momma, K. Nishimura, T. Tajima, J. Electrochem. Soc. 140 (1993) 2745–2748.
[105] K. Morigaki, N. Kabuto, K. Yoshino, A. Ohta, in: Proceedings of the 35th Battery Symposium (in Extended Abstracts), Nov. 14–16, 1994, pp. 83–84. Nagoya, Japan.
[106] M. Koltypin, Y.S. Cohen, B. Markovsky, Y. Cohen, D. Aurbach, Electrochem. Commun. 4 (2002) 17–23.
[107] R. Bhattacharyya, B. Key, H. Chen, A.S. Best, A.F. Hollenkamp, C.P. Grey, Nat. Mater. 9 (2010) 504–510.